Directional Dynamics of Fog: Irreversibility and Causal Coupling with Turbulence

Filippo Pesenti[1], Hossein Motalebi [1], Reban Niraula[1], Gabriel G. Katul[2], Kelly Y. Huang[1]

[1]University of Houston
[2]Duke University

Key Points:

- Fog intensity time series are time-irreversible.
- TKE leads fog intensity in formation, no clear lead–lag relationship exists in the mature stage, and fog intensity leads TKE in dissipation.
- In fog formation only, the strength of the fog series' irreversibility increases linearly with the strength of its causal linkage to TKE.

Corresponding author: K. Y. Huang, yhuang68@uh.edu

Abstract

Fog prediction remains challenging because the physical processes governing its lifecycle evolve across time scales and do not follow reversible or stationary dynamics. Using high-frequency observations from Sable Island, Canada, this study analyzes fog intensity and turbulent kinetic energy (TKE) for their time irreversibility and causal relations. Fog intensity exhibits temporal asymmetry in all stages, while TKE remains nearly reversible. The lead–lag structure between the two variables is stage dependent: TKE leads fog intensity during formation, the coupling becomes symmetric during the mature phase, and fog intensity leads TKE during dissipation. A notable result is during fog formation, the strength of fog's intrinsic irreversibility increases linearly with the strength of its causal linkage to TKE, revealing that fog initiation is governed by a directional sequence of turbulence–moisture interactions. These findings demonstrate that fog is a non-equilibrium, time-asymmetric system, and that capturing its stage-dependent directionality is required for enhanced fog prediction.

Plain Language Summary

Fog is difficult to forecast because it forms, matures, and dissipates through several different processes that do not behave the same way over time. Using new measurements from Sable Island, Canada, this study examines how changes in fog thickness relate to changes in the swirling motion or turbulence near the ground. Directionality in time is based on the conjecture that 'cause' must occur before or at the same time as the 'effect'. Using this conjecture, the analysis shows that fog development and decay have a preferred direction in time, and that the connection between fog and turbulence depends on the stage of the fog event. Before fog forms, changes in turbulence occur first. Once fog is established, the two evolve together with no clear leader. During dissipation, the sequence reverses so that changes in the fog occur before changes in turbulence. A key finding is that fog shows the strongest time-asymmetric behavior when turbulence has the strongest influence during formation. This finding implies that fog begins through a strongly directional chain of physical processes rather than through random fluctuations. Recognizing this stage-dependent directionality can improve future fog prediction methods and weather models.

1 Introduction

Fog is a near-surface meteorological phenomenon consisting of a suspension of water droplets that reduce the horizontal visibility below 1 km (WMO, 1996). Fog forms in various regions under a wide range of atmospheric conditions, and has profound impacts on transportation logistics, human safety, and ecological processes . Despite its importance, fog remains one of the most challenging atmospheric phenomena to predict, owing to the complex, multi-scale processes that govern its formation, duration, and dissipation (Bergot & Koracin, 2021; Gultepe et al., 2007). As a result, even high resolution weather models struggle to capture fog's formation and dissipation in real time (Steeneveld et al., 2015; Price et al., 2015; Hintz et al., 2024), underscoring gaps in fog dynamics and motivating new approaches.

Because fog exhibits strong intermittency and threshold-like behavior (Huang et al., 2023), a stochastic framework—already successful in rainfall studies—offers a promising avenue for advancing fog prediction. Rainfall has long been treated as a stochastic process in geophysics, with well-developed statistical models to represent its intermittent "on-off" behavior and intensity fluctuations (Peters & Neelin, 2006; Gaume et al., 2007; Rodriguez-Iturbe & Eagleson, 1987; Rigby & Porporato, 2010). Recent analyses have shown that fog event sequences share notable similarities with rainfall, such as comparable power-law statistics in the duration of dry periods and event sizes, as well as sim-

ilar spectral signatures in their on–off switching behavior (Räsänen et al., 2018). These parallels further motivate the development of stochastic models 'tailored' to fog.

A defining property of precipitation is its temporal irreversibility (also called time asymmetry), which reflects the inherent asymmetry between the rapid onset and gradual decay of storms, as well as the directional nature of moisture convergence, condensation, and runoff. Irreversibility in rainfall has been recognized as a critical property to incorporate into stochastic models (Molini et al., 2010), with Müller et al. (2017) showing that neglecting pronounced temporal asymmetry in synthetic rainfall series can bias hydrological applications, leading to errors such as overflow predictions in urban drainage.

Building on these outcomes, this study uses field data collected on Sable Island, Canada to investigate the temporal irreversibility in fog, an essential property to account for in the development of stochastic frameworks that capture fog's non-equilibrium dynamics. The analysis also links fog irreversibility to turbulent kinetic energy (TKE) – a known driver of the fog life cycle.

2 Methods of Analysis

2.1 Data

The datasets analyzed were collected on Sable Island, Canada, located off the coast of Nova Scotia (43.9337°N, 59.9149°W), over the month of July 2022 as part of the Fog and Turbulence Interactions in the Marine Atmospheres (FATIMA) – Grand Banks (GB) field campaign (Fernando et al., 2025). Over the observation period, fog occurred about 25% of the time. Time series of visibility (vis) was collected by a forward scatter sensor (Vaisala FD70) at a rate of 4 measurements per minute and a height of 2.5 m. Frequency components lower than 300^{-1} Hz in the fog time series were filtered out. To draw similarities with studies conducted on the intensity of rainfall (Molini et al., 2010), the intensity of fog is defined as

$$I_{fog} = \frac{1}{vis}, \tag{1}$$

such that lower visibility vis corresponds to a higher intensity of fog. The use of $1/vis$ as a surrogate variable for the intensity of fog is further motivated by parametrization studies that show $vis^{-1} \sim (N_d\ LWC)^{\gamma}$, where N_d is the number droplet concentration, LWC is the liquid water content, and γ is a constant around 0.5 (Gultepe et al., 2017).

Three-dimensional component wise velocity data were collected at 40 Hz with a sonic anemometer (Campbell Scientific IRGASON) located at a height of 2 m on the Center Tower (43.9337°N, 60.0224°W, which is approximately 20 m east of the FD70). Corrections to account for sonic path averaging and flow distortion by the sonic transducers are applied (Horst & Oncley, 2006; Horst et al., 2015), and frequency components lower than 300^{-1} Hz were filtered out. Turbulent kinetic energy (k) was then calculated as

$$k = \frac{1}{2}\left(\overline{(u')^2} + \overline{(v')^2} + \overline{(w')^2}\right), \tag{2}$$

where u', v', and w' are the longitudinal, transverse, and vertical velocity fluctuations, respectively, and overbar denotes time averaging such that k is down-sampled to 1/15 Hz to match the sampling rate of vis for calculations of cross correlations.

Sixteen fog events and one reference event with no fog were selected and listed in Table 1 and highlighted in Figure 1 (top). The fog events span a wide range of event lengths (from approximately 2 to 33 hours) and formation mechanisms (with the various synoptic set-ups included in Table 1). To examine how time irreversibility and its coupling with TKE evolve over the fog life cycle, each fog event was divided into formation, duration, and dissipation stages and analyzed separately. The formation stage encompasses fog onset and development, the mature stage covers the period of sustained fog (peak

Table 1. Observed fog events divided into the three stages (formation, duration, and dissipation). The corresponding intensive observation period (IOP) number for each event and the synoptic set-ups – high pressure (HP), low pressure (LP), mixing (MX), stable (ST), or CG (convergence zone) – are included. More details can be found in Fernando et al. (2025). All times are in UTC.

Event	IOP	Synoptic	Date	Formation	Duration	Dissipation
1	1	HP/MX	03/07/2022	01:35–10:24	10:24–11:38	11:38–11:55
2	2	CG/MX	07/07/2022	00:36–03:27	03:27–03:36	03:36–04:06
3	3	LP/ST	10/07/2022	05:18–05:43	05:43–06:45	06:45–07:14
4			10/07/2022	20:30–23:15	23:15–02:34^{+1}	02:34^{+1}–02:52^{+1}
0	4	LP/ST	13/07/2022	04:12–08:21	08:21–11:35	11:35–12:00
5	5	HP/MX	14/07/2022	01:07–02:51	02:51–09:43	09:43–10:16
6	6	HP/ST	15/07/2022	22:26–22:54	22:44–23:58	23:58–00:17^{+1}
7	7	HP/ST	18/07/2022	13:47–18:07	18:07–20:53	20:53–21:16
8	8	HP/ST	18/07/2022	21:17–04:14^{+1}	04:14^{+1}–15:15^{+1}	15:15^{+1}–15:40^{+1}
9	9	HP/ST	21/07/2022	20:29–22:52	22:52–13:43^{+1}	13:43^{+1}–14:14^{+1}
10	10	HP/ST	23/07/2022	21:35–22:26	22:26–13:15^{+1}	13:15^{+1}–14:02^{+1}
11			24/07/2022	20:38–21:07	21:07–04:37^{+1}	04:37^{+1}–05:50^{+1}
12			25/07/2022	19:03–20:40	20:40–22:08	22:08–22:36
13	11	CG/MX	26/07/2022	23:19–02:28^{+1}	02:28^{+1}–10:32^{+1}	10:32^{+1}–10:45
14	12	CG/ST	27/07/2022	22:39–01:29^{+1}	01:29^{+1}–05:46^{+1}	05:46^{+1}–12:48^{+1}
15	13	HP/MX	30/07/2022	03:21–04:08	04:08–11:43	11:43–12:22
16	14	LP/MX	31/07/2022	05:46–06:17	06:17–07:18	07:18–11:11

intensity and local steady state), and the dissipation stage marks the clearing phase. Accordingly, formation was identified as the period from when I_{fog} begins to rise until it stabilizes and plateaus, duration as the period where I_{fog} remains approximately constant, and dissipation as the period where I_{fog} begins to decrease until it reaches a minimum. To illustrate, Figure 1 (bottom) displays formation, duration, and dissipation stages for fog event 15 occurring on 30/07/2022.

2.2 Time Irreversibility

A time series Θ is time reversible if the joint probability distribution of any sequence of its values is identical to the joint probability distribution of that same sequence taken in reverse order. A series that does not have this property is considered irreversible, or directional, and its statistics depend on the direction of time (Lawrance, 1991; Zorzetto et al., 2018). Here, the time irreversibility of both the fog intensity and TKE series is evaluated using three complementary metrics: (1) the lag irreversibility, (2) the Kullback–Leibler (KL) divergence between forward and reverse joint distributions, and (3) the cross-scale correlation asymmetry in wavelet space.

In practice, evaluating reversibility through the full n-point joint distributions is infeasible given the rapid growth in dimensionality. A weaker but more practical diagnostic is the so-called lag reversibility, which only requires bi-variate joint probability distributions

$$p_{\Theta_t,\Theta_{t+\tau}}(\Theta_0,\Theta_1) = p_{\Theta_{t+\tau},\Theta_t}(\Theta_0,\Theta_1) \tag{3}$$

for all $\tau = 1, 2, ...$ and $t \in \mathbb{Z}$ (Lawrance, 1991). It then follows from lag reversibility that $\rho[\Theta_t^2, \Theta_{t+\tau}] = \rho[\Theta_t, \Theta_{t+\tau}^2]$, where $\rho[X, Y]$ denotes a correlation coefficient between variables X and Y. We define a lag irreversibility metric as (Zorzetto et al., 2018)

$$R(\tau) = \rho[\Theta_t^2, \Theta_{t+\tau}] - \rho[\Theta_t, \Theta_{t+\tau}^2] \tag{4}$$

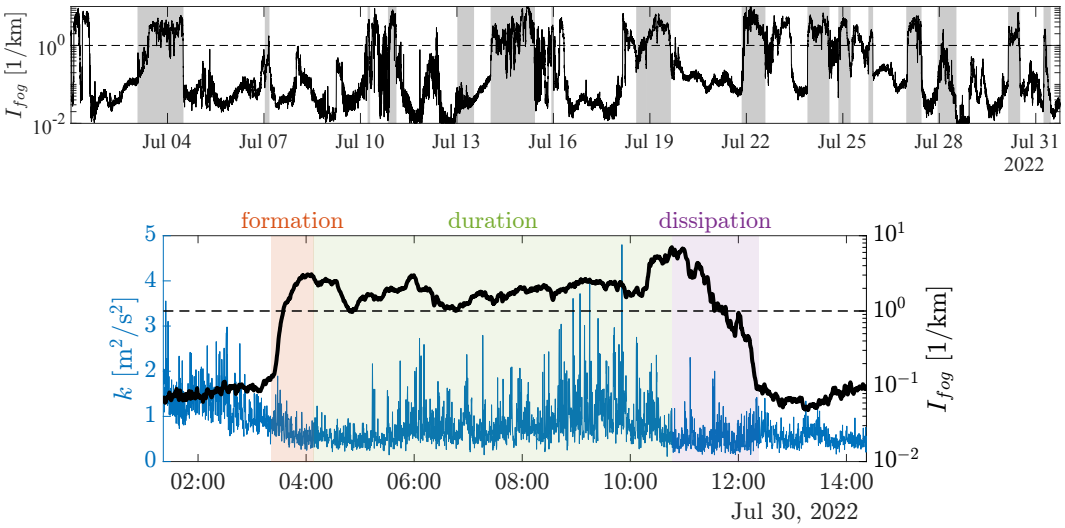

Figure 1. Top: Fog intensity for the duration of the FATIMA-GB campaign. Fog events selected are shaded in gray, including one reference event where no fog occurred. The horizontal dashed line represents a fog intensity of 1 km^{-1} (or a visibility of 1 km), consistent with the threshold above which fog occurs. Bottom: Turbulent kinetic energy k and fog intensity during the fog event 15 on 30/07/2022 to illustrate the division of the event into formation (orange), duration (green), and dissipation (purple) stages. The horizontal dashed line represents a fog intensity of 1 km^{-1} (or a visibility of 1 km) as before.

such that $R(\tau) = 0$ for a perfectly reversible process and $|R(\tau)| > 0$ otherwise.

Another measure of irreversibility is the Kullback-Leibler divergence (or relative entropy) between the forward and reverse joint distributions. This metric is derived from the fluctuation theorem and involves conditional probabilities of a variable and its first time-derivative (Porporato et al., 2007):

$$\langle Z_\tau \rangle = \int p_\Theta(\Theta) \int p_{\dot\Theta}(\dot\Theta|\Theta) \log \frac{p_{\dot\Theta}(\dot\Theta|\Theta)}{p_{\dot\Theta}(-\dot\Theta|\Theta)} d\Theta \; d\dot\Theta, \tag{5}$$

where the integrals extend over the whole domains of Θ and its time derivative $\dot\Theta$, which is approximated as $\Delta\Theta/\tau$. Similar to $|R(\tau)|$, $\langle Z_\tau \rangle = 0$ for a perfectly reversible process and $\langle Z_\tau \rangle > 0$ otherwise.

A third approach evaluated multiscale time directionality using a continuous wavelet transform (CWT) following Molini et al. (2010). The CWT decomposes the time series into scale-dependent coefficients from which local scale energies are derived. Directionality is then inferred from the asymmetry of the time-lagged cross-correlation between energies at adjacent scales: forward cascades yield stronger correlations at positive lags, inverse cascades at negative lags, and instantaneous processes produce symmetric correlations. However, as discussed later in the Results section, this approach is sensitive to the choice of wavelet basis and introduces smoothing through interpolation (continuous wavelet transforms produce high redundancy), so it is used only as a supplementary diagnostic.

2.3 Lead-Lag Relationships between Fog Intensity and TKE

Moving beyond the irreversibility in a single time series, the lead–lag relation between fog intensity and turbulent kinetic energy is examined through the asymmetry of

their cross-correlation, $\rho[I_{\text{fog}}, k]$. To preserve the low-frequency variability that is physically relevant to fog–turbulence coupling, cross-correlations were computed using the raw (non-detrended) I_f and k series. For any pair of variables X and Y, the cross-correlation is defined as $\rho[X, Y] = \text{Corr}\,(X(t+\tau), Y(t))$. While the peak magnitude reflects the coupling strength, the peak offset and resulting asymmetry encode causal directionality. A peak at positive τ indicates that $Y(t)$ correlates most strongly with future $X(t+\tau)$, implying that Y precedes X. Conversely, a peak at negative τ implies that X precedes Y. A symmetric $\rho(\tau)$ (peaking near $\tau \approx 0$) suggests no preferred lead–lag relation. The degree of this asymmetry can be quantified as:

$$A = \int \frac{\rho(\tau) - \rho(-\tau)}{\rho(\tau) + \rho(-\tau)} d\tau, \tag{6}$$

where $\rho(\tau)$ and $\rho(-\tau)$ represent the cross-correlation at positive and negative lags, respectively. The measure A is the integrated form of Q in Jachens et al. (2006). Cases where changes in TKE lead variations in fog intensity yield $\rho(\tau) > \rho(-\tau)$ and thus $A > 0$, whereas the opposite yields $A < 0$. The scalar metric A therefore condenses the full lead–lag dynamics into a single value, enabling direct comparison of the dominant causal direction across fog stages.

A more formal framework for interpreting this asymmetry is provided by linear response theory, which is used to describe the input-output properties of a system (Kubo, 1957). In this context, one variable is treated as an external perturbation and the other as the system's response. The asymmetry in their cross-correlation function then reveals the causal link, as a response cannot precede the action that causes it. The central tool for this analysis is the susceptibility, $\chi(\omega)$, which is the Fourier transform of the cross-correlation function:

$$\chi(\omega) = \int_{-\infty}^{\infty} \rho(\tau) e^{-i\omega\tau} d\tau \tag{7}$$

The susceptibility is a complex-valued function where the real part, $Re_{\chi(\omega)}$, corresponds to the symmetric (even) part of the correlation, and the imaginary part, $Im_{\chi(\omega)}$, corresponds to the asymmetric (odd) part (Borysov & Balatsky, 2014). Since causality is an inherently asymmetric, time-ordered concept, the imaginary part becomes the primary indicator for analysis.

The sign of the peak in $Im_{\chi(\omega)}$ for positive frequencies ($\omega > 0$) indicates the direction of the causal influence. Following the convention from applications in similar complex systems, a negative peak suggests that TKE acts as the input and fog intensity as the response (TKE $\rightarrow$ Fog). A positive peak suggests the reverse relation where fog intensity influences TKE (Fog $\rightarrow$ TKE). An imaginary part near zero would imply a symmetric relation with no clear lead-lag dynamic.

3 Results

3.1 Time Irreversibility

The lag reversibility metric $|R|$ and the Kullback-Leibler divergence $\langle Z_\tau \rangle$ are shown in Figure 2 (top and bottom rows, respectively) across the three life stages of fog. The absolute value of R is presented here to emphasize irreversibility magnitude, as its sign does not correspond to a physically interpretable direction. Fog intensity (colored lines) exhibits pronounced irreversibility, with both $|R|$ and $\langle Z_\tau \rangle$ significantly different from zero over a range of lags in all stages. In contrast, TKE (black lines) show $|R| \approx 0$ and $\langle Z_\tau \rangle \approx 0$ across all stages, indicating approximately time-reversible statistics consistent with an instantaneous cascade. This contrast implies that the irreversibility of the fog intensity signal is not simply inherited from the turbulent kinetic energy but arises from additional radiative and micro-physical processes governing fog evolution.

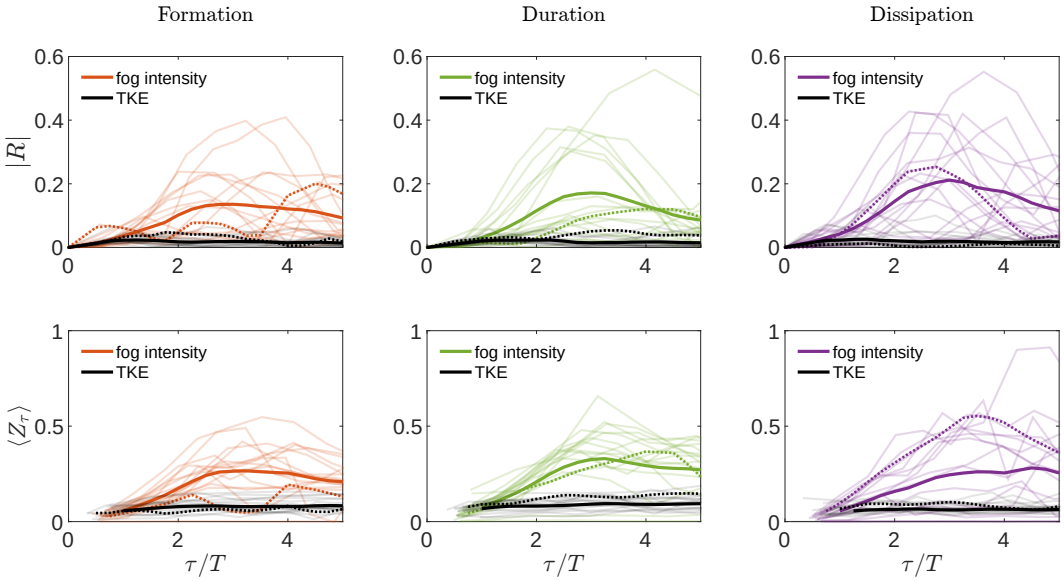

Figure 2. Lag reversibility metric $|R|$ (top row) and the Kullback–Leibler divergence $\langle Z_\tau \rangle$ (bottom row) as functions of normalized lag τ/T, where T is the integral time scale, for fog intensity (colored lines) and TKE (black lines) during the formation, mature, and dissipation stages of a fog event. Dark lines show the metric evolution averaged across all fog events, with individual events plotted as lighter lines. Dotted lines denote the reference no-fog case.

Time directionality is also assessed using the wavelet-based cross-scale representation, computed with the 4th-order Derivative of Gaussian (DoG) wavelet. Qualitatively, the fog intensity time series exhibits more temporal directionality than TKE in some events during the formation and dissipation stages, consistent with the results from the previous two metrics, although other events appear nearly symmetric. In the duration stage, most fog intensity cross-scale correlation functions are essentially symmetric, similar to that of TKE. The muted or symmetric wavelet-domain patterns likely result from the CWT's localization and redundancy, which smooth the signal and suppress low-frequency directional signatures. In the events that did exhibit a cascade direction, no consistent preference for forward or backward cascade direction is observed, with both directions occurring without an obvious connection to synoptic conditions. Moreover, the inferred cascade direction is sensitive to the choice of wavelet basis; in some cases a Morlet basis wavelet yields no or opposite signs of the asymmetry compared to the DoG basis wavelet. For these reasons, the time-domain metrics R and $\langle Z_\tau \rangle$ are treated as the primary indicators of irreversibility, and wavelet-based figures are provided in the Supporting Information.

3.2 Lead-Lag Relations between Fog Intensity and TKE

The cross-correlations between fog intensity and TKE are presented in the top rows of Figure 3 for each event and stage. For each stage, the solid colored line represents the averaged cross-correlation across all events, and the dashed line represents the reference no fog event. During the formation stage, a consistent positive asymmetry ($A > 0$) is observed across the fog events. This indicates that changes in k lead changes in fog intensity. This result is consistent with the physical understanding that a period of weakening turbulence is a necessary precondition for fog to develop, as calmer conditions allow for the local accumulation of moisture. For the duration stage, the relation becomes largely symmetric. This suggests a contemporaneous coupling, where the established fog

layer and the turbulence within it are in a state of quasi-equilibrium rather than a causal lead-lag dynamic (Dione et al., 2023). The causal direction reverses during the dissipation stage, which is marked by a clear negative asymmetry ($A < 0$), so that changes in fog intensity lead changes in TKE. Fog dissipation is often initiated by larger-scale phenomena such as changes in radiation or moisture availability. The subsequent breaking of the fog layer alters the stability of the atmosphere, which then enables new buoyancy-driven generation mechanisms that cause TKE to increase in response to the fog clearing (Dione et al., 2023).

Similar outcomes are seen in $Im_{\chi(\omega)}$, shown in the bottom row of Figure 3. During the formation stage, $Im_{\chi(\omega)}$ exhibits a negative peak in the positive frequencies, indicating that TKE leads fog intensity. This agrees with the positive asymmetry in the cross-correlation and reflects the role of weakening turbulence in enabling moisture accumulation. During the duration stage, $Im_{\chi(\omega)}$ generally fluctuates around zero with small amplitude, consistent with a largely symmetric and contemporaneous coupling between fog and TKE once the fog layer is established. In the dissipation stage, $Im_{\chi(\omega)}$ exhibits a positive peak for positive ω, indicating that changes in fog intensity precede changes in TKE. This frequency-resolved pattern mirrors the negative asymmetry observed in the cross-correlation and aligns with the physical picture in which fog thinning alters the local stability, enabling renewed turbulence production after the onset of fog erosion. Agreement between the time-domain cross-correlation and its spectral analogue is not unexpected given the Wiener–Khinchin theorem; however, such convergence formally requires approximate stationarity. Thus, the consistency between the two domains may be interpreted as indirect evidence that non-stationarity did not play a dominant role in this analysis.

3.3 Time Irreversibility and Causal Coupling with TKE

A notable relation emerges when the intrinsic time irreversibility of the fog intensity signal is compared with the strength of its coupling to TKE. Figure 4 shows that during the formation stage, both measures of irreversibility— integrated across five integral time scales to arrive at a single value for each fog event–increase linearly with the asymmetry measure A of $\rho[I_{fog}, k]$. Events in which TKE more strongly leads fog intensity (larger $A > 0$) also exhibit greater departure from time-reversible statistics. This coexistence of strong causal ordering and strong statistical irreversibility suggests that the physical processes governing fog initiation—particularly the rapid transition into a low-turbulence, moisture-accumulating regime—produce a pronounced temporal asymmetry in the fog evolution itself. This relation holds across all fog events, despite the wide range of synoptic setups and formation mechanisms (Table 1). In contrast, no such relation appears during the duration or dissipation stages, indicating that the linkage between causal influence and intrinsic irreversibility is specific to the onset of fog formation. This interpretation is consistent with a threshold-based role for TKE at the onset of dissipation: rather than acting as a continuous driver, a brief spike in turbulence may initiate the breakup of the fog layer, but it does not subsequently control the rate or structure of the decay.

4 Conclusion and Discussion

The fog life cycle was analyzed through the statistical lenses of time irreversibility and causal inference by examining sixteen fog events occurring on Sable Island, Canada, over the month of July 2022. The fog events spanned a wide range of synoptic conditions and formation mechanisms. Overall, fog intensity exhibits pronounced time irreversibility, whereas TKE remains nearly reversible across all stages of the fog life cycle. This contrast indicates that the directional structure in fog arises from thermodynamic and micro-physical processes rather than from turbulence energetics alone. The lead–lag

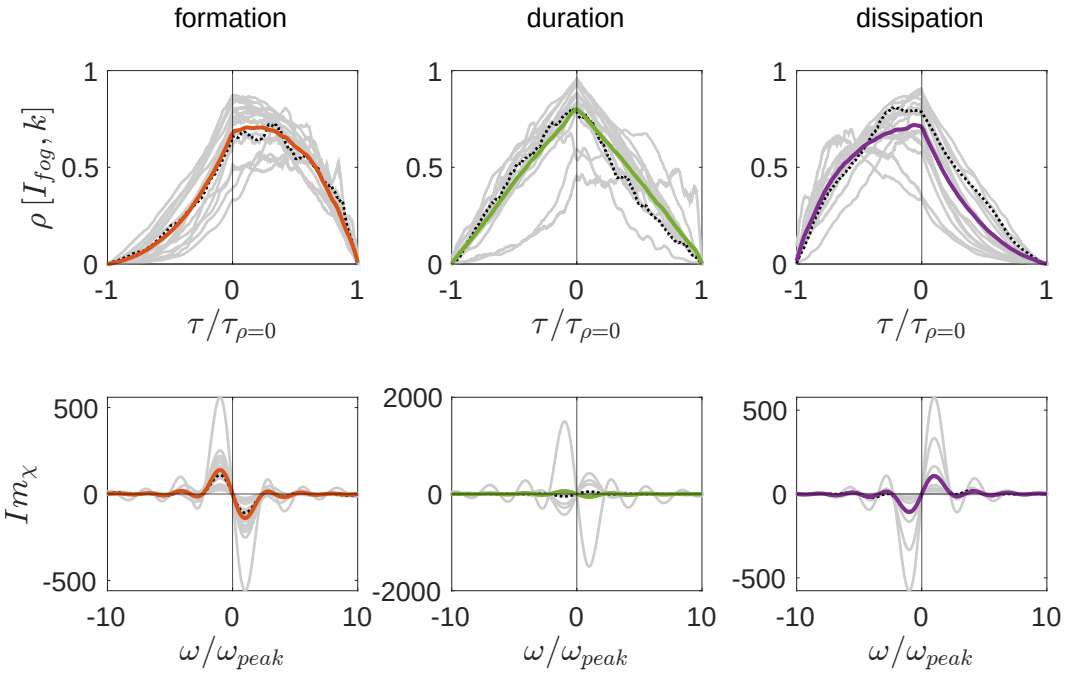

Figure 3. [Top row]: Cross-correlation, $\rho(\tau)$, between fog intensity (I_{fog}) and TKE (k) for the formation, duration, and dissipation stages. Grey lines represent individual fog events, colored lines the averaged $\rho(\tau)$ across all fog events, and the dotted lines the no-fog reference event. To highlight the asymmetry, the time lag τ is normalized by the time lag at which ρ crosses 0. [Bottom row]: Imaginary component of the corresponding susceptibility $Im_{\chi(\omega)}$. The frequency ω is normalized by the frequency at which the positive peak occurs. Grey lines show individual events, colored lines the mean across fog events, and dotted lines the no-fog reference.

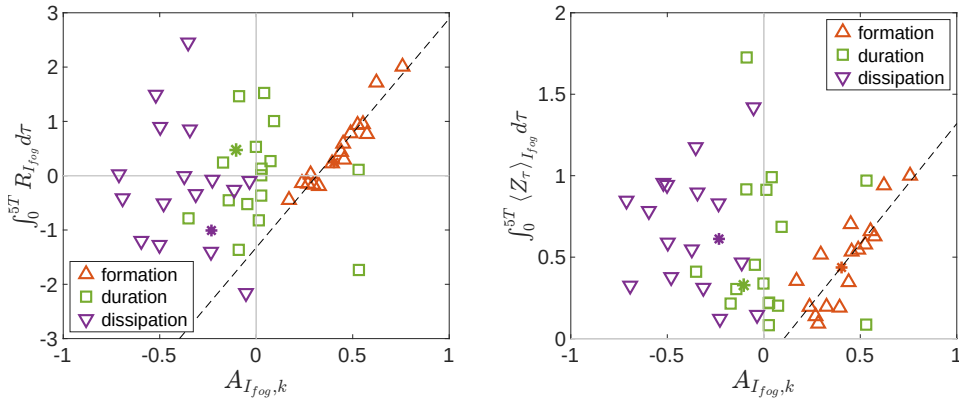

Figure 4. Time irreversibility of the fog time series based on R (left) and based on $\langle Z_\tau \rangle$ (right) versus the strength of TKE's causal influence (represented by A). To arrive at a single value representing the time irreversibility in each fog event, R and $\langle Z_\tau \rangle$ are integrated over $5T$, where T is the integral time scale. A linear relation, highlighted by the dashed lines, emerges in the formation stage for both metrics.

patterns between fog intensity and TKE further separate the stages: TKE leads fog intensity during formation, the coupling becomes largely symmetric during the mature stage, and fog intensity leads TKE during dissipation.

A key result is the emergence of a linear relation between fog's intrinsic irreversibility and the strength of its causal linkage to TKE only during fog formation. This alignment suggests that the onset of fog is governed by a directional sequence of turbulence–moisture interactions that imprint strong asymmetry on the fog signal. No such relation appears during duration or dissipation, consistent with quasi-equilibrium coevolution in the mature stage and with fog-driven stability changes dominating during decay. A brief turbulence spike may initiate breakup at the onset of dissipation, but it does not seem to govern the subsequent decay rate.

These results extend earlier work showing that fog evolves through irregular bursts rather than smooth transitions, revealing that fog is both intermittent and time-asymmetric (Huang et al., 2023). Taken together, these findings establish a quantitative view of fog as a non-equilibrium, directionally biased system whose stages are governed by different physical processes. Capturing this stage-dependent asymmetry will likely lead to improvements in fog prediction.

Conflict of Interest

The authors declare no conflicts of interest relevant to this study.

Data Availability Statement

The dataset analyzed is available at `https://github.com/atlas-uh/fog_directionality` for the peer review process, and will be permanently archived and assigned a DOI through Zenodo upon acceptance.

Acknowledgments
The field observations used in this study were collected during the FATIMA–Grand Banks campaign, supported by the Office of Naval Research under Grant N00014-21-1-2296 (FATIMA Multidisciplinary University Research Initiative) and administered by the Marine Meteorology and Space Program. Wavelet software was provided by C. Torrence and G. Compo, and is available at URL: http://paos.colorado.edu/research/wavelets/.

References

Bergot, T., & Koracin, D. (2021). Observation, simulation and predictability of fog: Review and perspectives. *Atmosphere*, *12*(2), 235. https://doi.org/10.3390/atmos12020235.

Borysov, S. S., & Balatsky, A. V. (2014). Cross-correlation asymmetries and causal relationships between stock and market risk. *PLoS One*, *9*(8), e105874. https://doi.org/10.1371/journal.pone.0105874.

Dione, C., Haeffelin, M., Burnet, F., Lac, C., Canut, G., Delanoë, J., ... Toledo, F. (2023). Role of thermodynamic and turbulence processes on the fog life cycle during sofog3d experiment. *Atmospheric Chemistry and Physics*, *23*(24), 15711–15731. https://doi.org/10.5194/acp-23-15711-2023.

Fernando, H. J. S., Dorman, C., Pardyjak, E., Shen, L., Wang, Q., Creegan, E., ... Yamaguchi, R. (2025). Fatima-gb: Searching clarity within marine fog. *Bulletin of the American Meteorological Society*, *106*(6), E971 - E1016. https://doi.org/10.1175/BAMS-D-23-0050.1.

Gaume, E., Mouhous, N., & Andrieu, H. (2007). Rainfall stochas-

tic disaggregation models: Calibration and validation of a multiplicative cascade model. *Advances in Water Resources*, *30*(5), 1301-1319. https://doi.org/10.1016/j.advwatres.2006.11.007.

Gultepe, I., Milbrandt, J. A., & Zhou, B. (2017). Marine fog: A review on microphysics and visibility prediction. *Marine fog: challenges and advancements in observations, modeling, and forecasting*, 345–394.

Gultepe, I., Tardif, R., Michaelides, S. C., Cermak, J., Bott, A., Bendix, J., ... COBER, S. G. (2007). Fog research: A review of past achievements and future perspectives. *Pure and applied geophysics*, *164*, 1121–1159. https://doi.org/10.1007/s00024-007-0211-x.

Hintz, T. J., Huang, K. Y., Hoch, S. W., Bardoel, S. L., Gaberšek, S., Gultepe, I., ... Fernando, H. J. S. (2024). A mechanism for coastal fog genesis at evening transition. *Q. J. R. Meteorol. Soc.*, *150*(762), 2727–2743. doi: https://doi.org/10.1002/qj.4732

Horst, T., & Oncley, S. (2006). Corrections to inertial-range power spectra measured by csat3 and solent sonic anemometers, 1. path-averaging errors. *Boundary-layer meteorology*, *119*(2), 375–395. https://doi.org/10.1007/s10546-005-9015-7.

Horst, T., Semmer, S., & Maclean, G. (2015). Correction of a non-orthogonal, three-component sonic anemometer for flow distortion by transducer shadowing. *Boundary-Layer Meteorology*, *155*(3), 371–395. https://doi.org/10.1007/s10546-015-0010-3.

Huang, K. Y., Katul, G. G., Hintz, T. J., Ruiz-Plancarte, J., Wang, Q., & Fernando, H. J. (2023). Fog intermittency and critical behavior. *Atmosphere*, *14*(5), 875. https://doi.org/10.3390/atmos14050875.

Jachens, A., Schumacher, J., Eckhardt, B., Knobloch, K., & Fernholz, H. (2006). Asymmetry of temporal cross-correlations in turbulent shear flows. *Journal of Fluid Mechanics*, *547*, 55–64. https://doi.org/10.1017/S0022112005007391.

Kubo, R. (1957). Statistical-mechanical theory of irreversible processes. i. general theory and simple applications to magnetic and conduction problems. *Journal of the physical society of Japan*, *12*(6), 570–586. https://doi.org/10.1143/JPSJ.12.570.

Lawrance, A. J. (1991). Directionality and reversibility in time series. *International Statistical Review / Revue Internationale de Statistique*, *59*(1), 67–79. https://doi.org/10.2307/1403575.

Molini, A., Katul, G. G., & Porporato, A. (2010). Causality across rainfall time scales revealed by continuous wavelet transforms. *Journal of Geophysical Research: Atmospheres*, *115*(D14). https://doi.org/10.1029/2009JD013016.

Müller, T., Schütze, M., & Bárdossy, A. (2017). Temporal asymmetry in precipitation time series and its influence on flow simulations in combined sewer systems. *Advances in Water Resources*, *107*, 56–64. https://doi.org/10.1016/j.advwatres.2017.06.010.

Peters, O., & Neelin, J. (2006). Critical phenomena in atmospheric precipitation. *Nature Physics*, *2*, 393–396. doi: https://doi.org/10.1038/nphys314

Porporato, A., Rigby, J. R., & Daly, E. (2007). Irreversibility and fluctuation theorem in stationary time series. *Physical review letters*, *98*(9), 094101. https://doi.org/10.1103/PhysRevLett.98.094101.

Price, J., Porson, A., & Lock, A. (2015). An observational case study of persistent fog and comparison with an ensemble forecast model. *Boundary-Layer Meteorology*, *155*(2), 301–327. https://doi.org/10.1007/s10546-014-9995-2.

Rigby, J., & Porporato, A. (2010). Precipitation, dynamical intermittency, and sporadic randomness. *Advances in Water Resources*, *33*(8), 923–932.

Rodriguez-Iturbe, I., & Eagleson, P. S. (1987). Mathematical models of rainstorm events in space and time. *Water Resources Research*, *23*(1), 181-190. https://doi.org/10.1029/WR023i001p00181.

Räsänen, M., Chung, M., Katurji, M., Pellikka, P., Rinne, J., & Katul, G. G. (2018). Similarity in fog and rainfall intermittency. *Geophysical Research Letters*, *45*(19), 10,691-10,699. https://doi.org/10.1029/2018GL078837.

Steeneveld, G., Ronda, R., & Holtslag, A. (2015). The challenge of forecasting the onset and development of radiation fog using mesoscale atmospheric models. *Boundary-Layer Meteorology*, *154*(2), 265–289. https://doi.org/10.1007/s10546-014-9973-8.

WMO. (1996). *Aerodrome reports and forecasts: a users' handbook to the codes.* Author.

Zorzetto, E., Bragg, A. D., & Katul, G. (2018). Extremes, intermittency, and time directionality of atmospheric turbulence at the crossover from production to inertial scales. *Phys. Rev. Fluids*, *3*, 094604. https://doi.org/10.1103/PhysRevFluids.3.094604.